7. STRUCTURAL AND ENVIRONMENTAL STUDIES OF ACOUSTICAL DUCT-LINING MATERIALS

By H. A. Watson, Jr., J. D. Thompson,
McDonnell Douglas Corporation

and

Carl E. Rucker
NASA Langley Research Center

SUMMARY

The structural design criteria for acoustical duct-lining materials depend on the interrelation of aerodynamic, acoustic, and environmental requirements. Environmental conditions are of more-than-normal concern in the design of inlet and fan exhaust ducts which incorporate acoustical materials since the environment is allowed to penetrate the porous facing.

The results of tests reported herein have shown that the acoustical-sandwich structural concepts are feasible. However, without further engineering research, the incorporation of a turbofan noise-suppression system will result in increased weight and complexity with probable loss of aircraft utility. Despite work accomplished to date in the field of structural and environmental testing of acoustical liners, a large amount of additional investigation remains in order to achieve the optimum structural design of a certifiable noise-suppression system for commercial aircraft.

INTRODUCTION

There is an immediate concern for reducing turbojet-aircraft noise which adversely affects the communities adjacent to commercial airports. One promising approach is the development of a noise-suppression system which may be applied to the inlet and exhaust ducts of turbofan engines. An acoustical system of this type requires that the internal wetted surfaces of the ducts be replaced by a porous sheet material backed by acoustical cavities. Honeycomb sandwich is an ideal structural configuration for such a system; but although the duct environment remains unchanged, the exposure of the porous surface, the honeycomb core, and the sandwich interior to the environment introduces a series of problem areas, including corrosion, contamination, and drainage. The subject of this paper will be confined to structural and environmental studies of materials proposed for

use as acoutical duct liners and to the tests, analyses, and design criteria necessary to provide a certifiable noise-suppression system for commercial aircraft.

SYMBOLS

a	acceleration, $in./sec^2$
dS	incremental change in stress
$d\epsilon$	incremental change in strain
EI	sandwich stiffness factor, $lb\text{-}in^2$
$E_T = \frac{dS}{d\epsilon}$	tensile modulus of elasticity, lb/in^2
$F_{t,u}$	tensile strength, lb/in^2
f	frequency, Hz (cps)
f_o	resonant frequency, Hz (cps)
g	acceleration due to gravity, 386 $in./sec^2$
L	length of beam, in. (also thickness or direction of core)
N	number of fatigue cycles to failure
R	stress ratio
S	stress, lb/in^2
T	thickness of core, in.
T_u	tensile ultimate stress, lb/in^2
T_y	tensile yield stress, lb/in^2
t	thickness of sheet or beam, in.

W width or direction of core, in.

A deflection, in.

E strain, μin./in.

P density, lb/in^3

ρ_p density of parent material, lb/in^3

DISCUSSION

General Considerations

Studies related to the structure and environment of duct-lining acoustical materials proposed for use in the noise-suppression system of turbofan aircraft may be more clearly understood when preceded by an explanation of the basic acoustical function of the materials and their location within the nacelle as well as a detailed description of typical duct-liner construction.

The materials discussed in this paper are those that are used primarily in tuned-absorber noise-suppression systems. Basically, these systems function as a series of dead-end labyrinths which, according to their design shape and volume, trap sound waves of a specified wave-length range.

The major noise sources within a turbofan engine are due to the rotating blades of the fan, compressor, and turbine (ref. 1); therefore, the acoustic traps are located within the inlet and exhaust ducts leading to and from these sources. A major restraint upon the noise-suppression system is that disturbances of the aerodynamic flow within the ducts should be minimal. Therefore, the noise traps are logically located flush with or beneath the wetted surfaces of the ducts. When large amounts of suppression are required, additional wetted surface areas, which may be acoustically treated, are usually provided by duct elongation or by the addition of rings, struts, and vanes as shown in figure 1.

A tuned absorber is a composite of sheet and cellular core materials stacked to form a single or multiple sandwich as shown in figure 2. In a single sandwich, the porous facing sheet forms the wetted surface of the treated duct. The cells of the honeycomb core, together with the solid facing sheet, form the dead-end traps. Structurally, the solid sheet acts as the pressure wall of the duct, but the total sandwich reacts imposed loads. In a double sandwich, composed of three facing sheets and two cores, any two of the facing sheets may be porous, according to design. The concentric rings of figure 1 are examples of one type of double sandwich in which the center facing sheets are solid

and the two outer facing sheets are porous, thereby forming two back-to-back simple absorbers. A second type of double sandwich is shown in figure 2. The exposed or wetted surface sheet and the center sheet are of porous material, and the bottom external sheet is solid. In this design, the depths or thicknesses of the two sandwiched cores are often different because they are tuned for different frequency ranges.

Acoustic-Panel Description

In a sandwich structure, the honeycomb core is comparable to the web of an I-beam, which supports the I-beam flanges and allows them to act as a unit. The web of an I-beam and the core of a sandwich carry the beam shear stresses. The core of a sandwich differs from the web of an I-beam in that the core provides continuous support of the facings and thus allows the facings to be worked up to or above their yield strength without wrinkling or buckling. In order that the sandwich will act as an integral unit, the weld or adhesive which bonds the core to its facings must be capable of transm'itting shear loads between the facings and, in the case of pressure loads, of also transferring flatwise tensile loads. The cellular structure of honeycomb core in the acoustic sandwich serves a dual purpose since it also provides the acoustic cavities. In the case of the multiple sandwich, as with the single sandwich, any differential pressure across the plane of the sandwich acts on the solid facing sheet but is reacted by the total sandwich.

In order to determine the structural characteristics of sandwich panels, the mechanical properties of the materials proposed as sandwich elements must first be determined. In the case of an acoustical sandwich, the four types of structural elements are (1) the porous facing sheets, (2) the solid facing sheets, (3) the honeycomb core, and (4) the bond or weld interface between core and facing sheets. (See fig. 3.)

Porous Facing Sheet Materials

Of the four structural elements, the one which presents the most difficulty in selection of material and configuration is the porous facing sheet. This component must be available in thin, formable sheet and have certain acoustic characteristics related to a uniform porosity or flow resistance (ref. 1). In addition, it should be capable of carrying imposed loads and must withstand the environment to which it is exposed as a duct-liner surface. Numerous types of porous facing sheets have been considered. Several of the more promising types are described and discussed briefly in the following paragraphs.

Perforated sheet.- As shown in figure 4, porosity may be accomplished by perforation of solid sheet materials with round holes. If perforated sheets prove to be acoustically acceptable, a multitude of perforated patterns and sheet materials are available for use.

Sintered fiber-metal sheet.- Fiber metal is a randomly interlocked structure of metallic fibers which are sintered to produce a microscopic weld at the fiber intersections, thereby forming an orthotropic three-dimensional truss. Examples of this material are shown in figures 5 and 6. The nose cowl inlet and fan exhaust ducts of the acoustically modified nacelle for the forthcoming McDonnell Douglas flight tests (ref. 2) were fabricated by using this type of porous facing sheet. Numerous types of this configuration are commercially available in sheet gages and fabricated of such materials as copper, silver, AISI types 430 and 347 stainless steel, and 17-4 PH stainless steel. The fiber diameters, dependent upon material, range from 0.0004 to 0.010 inch.

Sintered woven-screen sheet.- As shown in figure 5, sintered woven screen is a sintered composite of two or more finely woven metallic wire screens. These screens are produced in weaves such as plain, twilled, plain dutch, and dutch twilled. The mesh size may vary from 10 by 10 wires per inch to 400 by 2800 wires per inch. A wide variety of materials is available, including AISI types 304, 316, 321, and 347 stainless steel, monel, nickel, inconel, copper, and Hastelloy X. Figure 6 is a micrographic cross section of fiber metal with supporting top and bottom screens.

Sintered continuous-filament sheet.- As shown in figure 5, sintered continuous-filament materials are fine, continuous, unwoven metallic filaments which are sintered in a uniform mat. These sheets are available in the same materials and wire diameters as woven screens.

Woven fiber-glass sheet.- Woven fiber glass (fig. 5) is a woven cloth of fiber-glass filaments available in a wide variety of weaves. With the proper resin matrix and layup methods, this material can be used to produce porous sheets. The porosity may be produced by control of the resin content or by mechanical molding of holes during resin cure. A polyimide resin system may provide a fiber-glass-reinforced structure which will withstand a continuous temperature of 500° F.

Solid Facing Sheet Materials

In the acoustical sandwich panel, the solid facing sheet is the pressure wall of the structure. Therefore, the gage and material of the solid facing are selected to withstand the hoop-tension loads of the duct.

Core Materials

Cellular cores yield the highest strength-to-weight ratio of all geometric structures. Honeycomb core is a lightweight structure of thin ribbons which are bonded or welded at nodes to form, when expanded, any of a large variety of cell sizes and cell shapes, such as squares and hexagons. The cell size is the diameter of an inscribed

cylinder. The ribbon of honeycomb core may be paper, plastic, fiber glass, metal, or any of a vast number of other materials. Figures 2 and 3 illustrate hexagonal and sine-wave cores, respectively. The core used in the fabrication of the McDonnell Douglas flyover nacelles (ref. 2) has a cell size of 0.75 inch, is of sine-wave configuration, and has been grooved for drainage as shown in figure 3. The ribbon is a heat-resistant phenolic resin system reinforced by woven fiber-glass fabric. In the case of welded metallic cores, one unique design with ribbon flanges welded to the facings is shown in figure 7.

Adhesive and Weld Materials

As previously stated, the honeycomb core must be capable of transmitting shear and flatwise tensile loads between the sandwich faces. The dual functions of the acoustic honeycomb sandwich, that is, acoustic attenuation and structural support, require exacting control of the adhesive bonding or weld interface between the honeycomb core and the porous facing sheet. The design objective has been to obtain an adhesive fillet between the honeycomb core and the porous facing which would be structurally adequate (300 psi in flatwise tension) with a minimum blockage of the porous facing material. (See fig. 8.)

In the McDonnell Douglas design of ground- and flight-test hardware described in references 1 and 3, it was found that commercially available structural bonding systems did not have the desired filleting action during cure and that standard adhesive-application methods did not provide uniform distribution of the bonding materials on the ribbon of the core. The solution of the problem involved the adaptation of a carrier-supported, aluminum-filled, modified-epoxy, film adhesive. The unique adaptation involved elimination of the scrim-cloth carrier and revision of the method of applying the adhesive to the core. The materials used in the bonding process are illustrated in the exploded view of the sandwich as shown in figure 9. The bonding method is shown in figure 10 and described in the following steps:

(1) A sheet of adhesive film is detached from its polyethylene separator and spread over the surface of the honeycomb core.

(2) The adhesive is caused to coagulate at the core ribbon by application of localized heat with a heat gun or heat lamp.

(3) The adhesive-core subassembly is then inverted onto the aluminum sheet, bagged, and cured for 1 hour at 350° F in a vacuum of 10 psi. (The term "bagged" refers to enclosing the bonding assembly in a flexible plastic bag and drawing a vacuum to obtain an elastic clamping of the assembly during oven cure.)

(4) When the sheet-adhesive-core subassembly has cooled, adhesive film is spread on the exposed surface of the core, coagulated at the core ribbon by localized heat, as in steps (1) and (2), and allowed to cool.

(5) The porous acoustic facing is then positioned. This operation is not critical since the adhesive hardens after cooling, is not tacky, and does not smear.

(6) The final assembly is bagged and cured for 1 hour at 350° F in a minimum vacuum of 10 psi. The pattern of the bondline is usually visible on the exterior surface of the porous facing material.

In duct areas with elevated temperatures, welded honeycomb becomes a candidate material for the acoustic sandwich. Figures 11 and 12 are micrographic studies of porous sheet welded to metallic ribbon; the material is stainless steel.

Environment

Acoustic requirements dictate that porous surfaces backed by air cavities be used as inlet and fan-exhaust-duct internal surfaces. Thus, the surfaces are structurally more complex than usual and typically require materials, processes, and structural concepts which are not conventionally used for these applications. As a result, particular attention must be paid to the environment in which the acoustic absorbent liners must function.

In the air-intake duct, the treated structure will be exposed to pressures, relative to ambient, ranging from -3 to 4 psi during normal usage. Indications are that on rare occasions of violent engine surges, pressures may peak at values of 15 to 40 psi. Sound pressure levels in the inlet are known to approach 175 dB at high power settings. Treated cowl surfaces will be exposed to atmospheric temperatures ranging from -85° to 125° F or higher. Within the nose-cowl structure, temperatures will commonly be several hundred degrees Fahrenheit, and hot anti-icing plumbing will locally subject surfaces to temperatures of nearly 450° F. In the case of a failed temperature-control valve, temperatures ranging up to 750° F could be encountered locally. In flight operations, the orientation of the engine inlet to oncoming airflow will expose the treated structure to the erosion or damage of rain, hail, and birds and, during ground operations, to the damage of pebbles, slush, and debris.

The fan exhaust ducts must withstand pressures up to 15 psig. Fan-air temperatures will range from about -65° to 250° F. Air velocities within the duct will vary from Mach numbers of about 0.4 to 1.0 between the entrance and exit sections at cruise conditions. Since the ducts form part of the enclosure surrounding the engine compressor case and accessory section, the treated surfaces in this area will be exposed to temperatures within the nacelle which are nominally 300° to 350° F. Locally, compartment

temperatures range up to 750° F near bleed-air piping, where high-pressure leaks may occur. In the event of a fuel fire, temperatures over 2000° F could be encountered. If a fire is started, it is desirable that burnthrough of the fan ducts not occur rapidly. Fire resistance should permit ample time for fire detection and for corrective action to be taken before burnthrough could occur and result in pressurized fan exhaust air being fed to the fire. In concepts featuring long ducts with treated surfaces facing the engine case aft of the compressor section, the treated liner must cope with heat radiation of temperatures up to 1400° F.

The phenomenon of subsurface recirculation losses in the air inlet and fan exhaust ducts is of interest to the power-plant performance engineer. Since the liner surface must be porous and backed by air cavities, and since wall static-pressure gradients exist in the inlet and exhaust flow paths, each cavity has a flow of air entering through regions of high surface pressure and leaving through regions of low surface pressure. There is a resulting small loss of momentum which is additive to the friction loss of the treated surface. Experience has shown that if cavity lengths are kept small, that is, less than 2 inches in the direction of the pressure gradient, the subsurface recirculation losses are small compared with friction losses.

An item which has been of little or no concern in the past, but which is of great concern to the designer of acoustically treated ducts, is porous-surface contamination. Figure 13 illustrates a typical time history of the in-service exposure of a large commercial transport aircraft to various potential contamination conditions.

On the ground, contamination conditions include exposure to oil, solvents, grease, and dirt during maintenance operations. During engine run-up and taxi, treated surfaces will be in the presence of exhaust products, dust, vapors, ground debris, slush, and water. One condition of concern is due to the frequently recurring situation of aircraft lined up awaiting take-off. During this wait, the engines are operating on air mixed with exhaust products from the aircraft ahead. The accumulation of solid particulate matter and vapor in the porous liner surfaces may become significant.

During flight, the treated liners will be exposed to water in the form of solid, liquid, and vapor. Smog and dust will be encountered at low altitudes. Collection of radioactive dust may be of concern at high altitudes. Experience with filters in current aircraft air-conditioning systems has indicated significant collection of radioactive materials. In most types of liners, it may be necessary to include provisions for water drainage from air cavities to protect against loss of sound-absorption qualities, damage due to freezing and expansion within cavities, and weight penalties caused by undrainable water.

Mechanical-Properties Testing

A complete compilation of the mechanical-properties testing performed to date on the noise-alleviation materials proposed for use in noise-attenuation programs is not within the scope of this paper. Therefore, an outline of the tests necessary to determine design allowables for these materials and pertinent data presently available will be presented.

Because the porous sheet materials (particularly the woven and fiber configurations) and the honeycomb core have properties which vary with the direction in the material, they are defined as orthotropic materials (ref. 4). The structural theories of homogeneous, isotropic materials do not apply to orthotropic materials without major revision; but this subject will not be explored in this discussion. However, it may be noted that in order to determine the mechanical properties of isotropic materials, tests along the longitudinal and transverse axes are required, whereas with orthotropic materials, a third test along a diagonal axis is also required in order to define fully the mechanical properties. Figure 14 is a polar orientation plot of fiber-metal tensile strength along three axes.

A component listing of mechanical-properties tests necessary to provide design allowables for noise-alleviation configurations is presented. Tests which are underlined require room temperature, elevated temperature, and special environmental testing.

(1) Porous sheet materials

(a) Tensile tests along three axes to determine tensile yield, tensile ultimate, elongation, and modulus of elasticity (ref. 5)

(b) Flexural fatigue tests along three axes to determine flexural endurance strength (ref. 6)

(c) Interlaminar shear tests along three axes to determine shear strength of resin system or shear strength of sintered fibers (ref. 7)

(d) Bearing tests to determine tear-out shear or bearing strength when sandwich is loaded by mechanical fasteners or rivets (ref. 8)

(e) Photoelastic tests of perforated sheets under biaxial loading to determine stress concentration factors due to hole pattern

(2) Core materials (honeycomb, etc.)

(a) Flatwise tensile tests to determine core tensile strength, usually combined with adhesive or weld test to insure attachment develops full strength of core (ref. 9)

(b) Flatwise compression tests, with specimens bare and supported, to determine strength of core. This test determines the strength loss due to the drainage grooves (ref. 9).

(c) Core shear tests along two or three axes, according to sandwich design. The complete sandwich is usually tested to determine the shear strength of the adhesive or weld (ref. 9).

(3) Adhesive or weld system

As previously outlined, the adhesive or weld system is usually tested in flatwise tension and shear as a component of the total sandwich.

Preliminary lap shear tests are required to determine adhesive-strength allowables. As a special consideration for acoustical sandwich designs, tests are made at elevated temperatures and pressures to determine also the effects of accelerated oxidation and the quality of protective coatings.

(4) Composite sandwich

(a) Flexural beam tests along three axes to determine stiffness factors of the sandwich and compressive buckling allowable of the porous facing sheet (ref. 9)

(b) Flexural fatigue tests of symmetrical beams along three axes to determine flexural endurance strength of the total sandwich. Symmetrical beams are .sandwich panels with equal facing sheets on the exterior surfaces and symmetrical construction about the neutral axis of the panel.

(5) Mechanical fasteners

Fastener tests are made along design axes to determine attachment strength of potted or welded inserts or other mechanical fasteners.

Testing at NASA Langley Research Center. - Flexural fatigue tests of fiber-metal sheet materials were performed at NASA Langley Research Center. The specimens in these tests were fabricated from commercially available AISI 347 stainless-steel fiber-metal sheets. The density of the parent material is 0.29 lb/in^3, the tensile modulus of elasticity is 28.0×10^6 lb/in^3, the tensile ultimate is 9.0×10^6 psi (bar annealed), and the endurance limit is 3.9×10^4 psi (annealed). AISI 347 is an austenitic-type (nonhardenable) stainless steel.

The fibers were tooled to random lengths from 0.0028-inch-diameter wire, bonded together in sheet configurations by heating in a reducing atmosphere (sintered), and formed to the correct volume (thickness) and density. The densities of the materials

tested were 40, 55, and 70 percent of the density ρ_p of an equal volume of the parent material.

Sixteen tensile coupons and 44 fatigue coupons were cut from four 12.5- by 16- by 0.060-inch commercially available fiber-metal sheets. Each sheet was cut into 11 fatigue coupons (seven from the longitudinal direction and four from the transverse direction) and four tensile coupons. Electrodischarge machining was used to cut the specimens (holes included) directly from the sheets. This machining technique resulted in excellent edge conditions, with fibers left relatively undisturbed adjacent to the cut. Fatigue coupons were selected in a random manner to prevent biasing of data due to sheet selection and longitudinal or transverse specimen orientation. Twenty-two fatigue coupons were allocated to these tests, but not all these coupons were tested. Sixteen tensile specimens were tested for each density of fiber metal. Two longitudinal and two transverse coupons were taken from each of four sheets.

Standard tensile tests were run on a conventional hydraulic load machine. An extensometer of 1-inch gage length was used to measure strain. Load-strain curves were recorded on an x-y plotter.

Load-strain curves were obtained from tensile tests, and ET, T_u, and T_y were determined. A sample stress-strain curve for supported fiber metal (based on measured specimen areas and load-strain curves) is shown in figure 15. The tensile modulus of elasticity E_T is defined as the slope of the straight-line portion of a stress-strain curve. The following values of E_T were obtained: 1.91×10^6 for 40-percent ρ_p, 3.01×10^6 for 55-percent ρ_p, and 8.83×10^6 for 70-percent ρ_p.

A 50-lbf electrodynamic shaker system, as shown in the photograph of figure 16, was used to test the 40- and 55-percent-density material specimens. The specimens were mounted as cantilever beams. The 70-percent-density material specimens were tested in the same manner, except that two 50-lbf electrodynamic shakers were operated in tandem and the test specimens were mounted on a yoke between the two shakers. An oscillator was used to set the driving frequency and amplitude.

At the beginning of each test, the driving frequency was increased from a relatively small amplitude in order to determine the first natural bending vibration mode of the specimen. The fatigue tests were then accomplished at the beam natural frequency at various root-stress levels.

The stress levels were determined by means of the output of a piezoresistive or piezoelectric accelerometer on the end of the beam. The specimens were tested over a range of accelerations. In all cases, acceleration measurements were better than ±3-percent accurate.

The specimens were tuned to resonance f_o by monitoring the tip accelerometer at very low loads. The peak deflection A and the peak acceleration a are then related by the following formula:

$$a = 0.102\ f^2\ A$$

The beam was assumed to be a constant-strength beam with stress S related to deflection by

$$\Delta = \frac{SL^2}{E_T t}$$

where L is the length of the beam, t is the thickness of the beam, and E_T is the tensile modulus of elasticity. For these studies, the thickness t was 0.060 inch, the length L was 4.3 inches, as indicated by figure 17, and E_T was determined by averaging data from several tensile tests.

Supplementary instrumentation included a strain gage (single) located at the root of the beam and a reference piezoelectric accelerometer located on the base clamp which held the test specimen.

Test data were monitored by root-mean-square voltage to direct-current converters (voltmeters). The output strain and output tip acceleration analog signals were monitored on a strip-chart recorder. The input frequency was measured from the oscillator on a frequency counter, and the number of cycles accumulated was measured from the tip accelerometer by a counter in the continuous counting mode.

At the start of the test, acceleration was increased quickly to the desired level and was held essentially constant (typical variation was ±0.5g, rms) for the duration of the test. As the test progressed, there was indication that the natural frequency of the model decreased, probably because of reorientation of fibers, fracture of fiber bonds, breaking of fibers, or some combination of these phenomena. These changes of the fibers resulted in a lowering of the resonant frequency, and thus the driving frequency was readjusted to the resonance value. Frequent adjustments of the input frequency and the tip acceleration as the beam stiffness decreased resulted in an essentially constant loading force and constant root strain by comparison with the acceleration and strain records. Although the deflection increased as a function of time, readjustments of input frequency and tip acceleration resulted in an essentially constant root strain.

The endurance limit, which is the limiting value of the stress below which the material can presumably endure an infinite number of stress cycles (where the S-N curve becomes horizontal), was determined from figure 18. As an example, an endurance limit of 1500 psi was determined from 16 tests of the 40-percent-ρ_p material, an endurance

limit of 2600 psi was determined from nine tests of the 55-percent-ρ_p material, and an endurance limit of 7600 psi was determined from 17 tests of the 70-percent-ρ_p material. Fatigue curves from figure 18 show that fatigue strength decreases rapidly as density decreases.

Testing at McDonnell Douglas, Long Beach and Santa Monica.- To date, the mechanical-properties testing at McDonnell Douglas has been concerned with determining the strengths of the acoustic materials involved in the design of the NASA Langley flight-test nacelles. (See ref. 2.) The interim results of this program are presented in tables I to VII and figures 14 and 19. These tests were performed according to the test methods indicated in the previous section.

The absence of an acceptable inspection method for bonded honeycomb structure and the necessity of a sonic fatigue environmental test of the inlet and fan exhaust ducts have combined to produce a comparative fatigue test which has proved to be an excellent method of detecting flaws in bonded structure and a flexural fatigue method of comparing the relative endurance of honeycomb-sandwich structure.

Testing was conducted by the Acoustics and Dynamics Environmental Laboratories of the Engineering Laboratory and Service (EL&S) Department of the Missiles and Space Systems Division of the Douglas Aircraft Company. The test facility used consisted primarily of a progressive wave tube (PWT), a bank of 10 Ling electropneumatic transducers coupled to 10 Ling exponential horns 72 inches *long,* a Cooper Bessemer motor-driven air compressor, and an instrumented control room. The PWT, constructed of 0.5-inch-thick sheet steel plates, was 6 inches wide and capable of accommodating test panels as large as 5 by 10 feet. This high-intensity sound system (HISS) was housed in a building constructed of 12-inch-thick concrete walls.

The fatigue resistance of the acoustically treated panel designs tested was evaluated by comparing the test conditions which caused the panels to fail, that is, the overall sound pressure level (OASPL) of the excitation that caused the initial failure, the approximate length of time the panel was exposed to the OASPL, and the extent of damage incurred. The spectrum of the sound pressure level (SPL) used to excite the test panels simulated, for the most part within i 2 dB from 50 to 800 Hz, the SPL existing at the walls of the inlet and fan exhaust ducts attached to a JT3D fan-jet engine operating at take-off power. The average spectrum was determined from measurements at five microphone locations. It was not possible to alter the level of the 80-Hz peak and the 125-Hz dip to produce a more uniform distribution without significantly changing the entire spectrum because of the inherent nature of the HISS. Typical variations in OASPL over the surface of each test panel were about i1 dB.

Each panel was subjected to an QASPL of 150 dB for a period of 2 hours and thereafter, to a series of 1-hour exposures to OASPL's varying from 153 dB to the maximum output capability of the HISS (165 to 166 dB), in 3-dB increments until failure occurred or until a total of 10 hours of sonic-fatigue-free time (including the initial 2 hour's of exposure to 150 dB) had been accumulated. Periodically, the tests were stopped and the panels were visually inspected for signs of fatigue. The inspection intervals varied somewhat with each test panel and with the nominal QASPL.

The test panel was mounted in the wall of the PWT and held in place with 0.25-inch-diameter bolts spaced 4 inches on center along the horizontal edges and with U-shaped clamps along the vertical edges. The U-shaped clamps along the vertical edges of the test panel were also bolted to the wall of the PWT (but not through the test panel) with 0.25-inch-diameter bolts spaced 4 inches on center. In order to ensure a smooth and continuous transition between the inner surface of the PWT and the surface of the installed test panel, the small gaps (0.1 to 0.2 inch in width) between the horizontal edges of the panel and the inner surface of the PWT were filled with putty; the larger gaps (0.5 to 1.25 inches in width) between the vertical edges of the panel and the inner surface of the PWT were stuffed with a solid foam plastic. All skin and rib panels were installed in the PWT so that the Z-frame with the most closely spaced rivets was closest to the sound source.

A portion of the wall of the PWT opposite the wall to which the test panels were mounted was replaced by a 48- by 96-inch sheet of 0.75-inch-thick plexiglass to permit visual inspection of the acoustically treated surface of the test panels. Typical damage due to high-intensity sound is shown in figure 20.

Environmental Testing

Rectangular-duct (exhaust-soot) test. - Since the rate, degree, and physical characteristics of liner clogging due to sooting (while aircraft operate in close proximity awaiting take-off) are unknown, an experiment is being performed with the apparatus shown in figures 21 and 22. Six disk-shaped specimens of treated construction may be fitted into the test flow duct. The specimens are located in various positions with respect to the flow passing through the duct. For instance, some are placed parallel to the duct center line, while others are positioned on surfaces inclined into or away from the flow. In addition, some are located in a constant-area duct section, while others are in areas of effusion or diffusion such that pressure gradients are imposed and subsurface recirculation is induced.

In general, the test procedure is to position the test duct, with specimens installed, about 100 feet behind ground run-up locations such that the duct is alined with a turbofan-engine exhaust. A log is maintained to record time exposure to engine exhaust flow at

high and low powers. Periodically, the specimens are removed for inspection. Flow-resistance measurements are made and the specimens are examined microscopically. Although the actual aircraft in-service environment is not simulated, these tests will provide qualitative information in the following areas:

Identification of contaminates

Relative clogging rates of forward-facing, tangent, and aft-facing surfaces

Relative clogging rates in effuser, constant-area, and diffuser sections

Relative clogging of various surface materials

Clogging rate, oil-film aggravation, and mechanisms of clogging

Effect of subsurface recirculation upon clogging

In-service structural and contamination evaluation of acoustic materials.- Various airline operators have expressed an interest in the development, handling, and maintenance of acoustic liner materials. As a result, a program has been initiated by Douglas and several cooperating airlines to install test specimens of acoustic-material construction within the fan exhaust ducts of operational Boeing 720B airplanes. The installations of these specimens are shown in figures 23 and 24.

An existing removable panel (fig. 25) has been modified to accept two specimens which are approximately 8 inches in diameter. The specimens are removable and are periodically returned to Douglas for examination. They are visually inspected for structural damage and subjected to flow-resistance tests to determine the degree of contamination or clogging. In addition, each specimen is carefully weighed and, should a specimen be damaged, a micrographic study is performed. After inspection, the specimens are returned to the airline and reinstalled in a fan duct for continued environmental exposure.

It is anticipated that this program will provide basic data for a better understanding of the performance of several types of liner construction in terms of contamination rate and structural integrity in an environment of actual operation. Two fiber-metal honeycomb specimens have been returned to Douglas for initial inspection after 198 flight hours of exposure in the Western United States, Mexico, and Canada. No significant damage or clogging was noted, although the exposed surfaces showed some discoloration. In the near future, interwoven polyimide-fiber-glass specimens and welded stainless-steel specimens will be introduced into the program.

Water-drainage tests.- In typical applications of acoustical liners, the probability exists that water or other liquids will collect within the resonant cavities, particularly where the porous liner surface is oriented upward as, for instance, in the lower section of the inlet duct. Analysis of a DC-8 nacelle modified to incorporate sound-absorbing

ducts indicated that approximately 100 pounds of water could be trapped. Because of concern about corrosion, loss of sound-absorption qualities, and added weight to the airplane, it is desired that provisions for overboard drainage be incorporated.

To resolve this problem, a subscale drainage fixture (fig. 26) was built and tested. The fixture featured a typical sandwich composed of a fiber-metal facing sheet, a 0.75-inch cell with a depth of 0.75 inch, and a solid aluminum backing sheet. Drainage passages to interconnect cells were formed by notching the honeycomb with slots 0.125 inch wide and 0.25 inch deep. Care was taken to form interconnections circumferentially rather than longitudinally so that water could drain downward. Longitudinal interconnections were avoided because significant wall pressure gradients exist in that direction within the duct and damming of the cavities is required to prevent subsurface air recirculation. A manifold, by which liquid could be collected from each row of slots and drained overboard, was provided at the bottom of the fixture.

In tests of the fixture under simulated rain conditions, it was determined by weight evaluations that drainage effectiveness was about 65 percent for this particular liner construction and drainage concept. Failure to achieve complete drainage resulted primarily from an inability to position the drainage passage at the lowest physical level in each honeycomb cell. If structural considerations permit, the drainage slots should be properly located.

Panel burnthrough test.- Figure 27 shows results of a burnthrough test of an 8- by 8-inch panel constructed of 0.75-inch fiber-glass honeycomb sandwiched between a fiber-metal porous surface and a 0.25-inch laminated-fiber-glass backing sheet. This panel construction is similar to the fan-duct liner construction to be used in the flight-test program of reference 2. When exposed to a 2000° F flame, the 0.25-inch fiber-glass backing sheet resisted burnthrough for 9 minutes. This was considered to be adequate for the limited flight-test program. For production applications, however, a 15-minute burnthrough resistance is required, as mentioned earlier, to provide ample time for fire recognition and corrective action in the event of an accessory-section fire.

CONCLUDING REMARKS

The structural design criteria for acoustical duct-lining materials depend on the interrelation of aerodynamic, acoustic, and environmental requirements.

The results of tests reported herein have shown that the acoustical-sandwich structural concepts are feasible but that further intensive engineering research is required before such concepts can be safely employed in commercial aircraft.

Two of the important items that need further research are the effect on the fatigue life and the corrosion of the duct-lining structure caused by permitting the honeycomb core and the backing structure to be exposed to the environment because of the porosity of the facing sheets. Additional engineering research must also deal with the problems of inspection, maintenance, and repair that are brought about by complex sandwich structure, as well as with the problem of weight that is in excess of the minimum required for acceptable fatigue life.

REFERENCES

1. Mangiarotty, R. A.; Marsh, Alan H.; and Feder, Ernest: Duct-Lining Materials and Concepts. Conference on Progress of NASA Research Relating to Noise Alleviation of Large Subsonic Jet Aircraft, NASA SP-189, 1968. (Paper No. 5 herein.)

2. Coxon, J. S.; and Henry, C. A.: Flight-Test Nacelles. Conference on Progress of NASA Research Relating to Noise Alleviation of Large Subsonic Jet Aircraft, NASA SP-189, 1968. (Paper No. 11 herein.)

3. Marsh, Alan H.; Zwieback, E. L.; and Thompson, J. D.: Ground-Runup Tests of Acoustically Treated Inlets and Fan Ducts. Conference on Progress of NASA Research Relating to Noise Alleviation of Large Subsonic Jet Aircraft, NASA SP-189, 1968. (Paper No. 10 herein.)

4. Faupel, Joseph H.: Engineering Design. John Wiley & Sons, Inc., c.1964.

5. Anon.: Tentative Method of Test for Tensile Properties of Plastics. ASTM Designation: D 638-67 T. Pt. 27 of 1968 Book of ASTM Standards With Related Material. Amer. Soc. Testing Mater., 1968, pp. 189-202.

6. Anon.: Tentative Methods of Test for Repeated Flexural Stress (Fatigue) of Plastics. ASTM Designation: D 671-63 T. Pt. 27 of 1968 Book of ASTM Standards With Related Material. Amer. Soc. Testing Mater., 1968, pp. 217-234.

7. Anon.: Plastics: Methods of Testing. Fed. Test Method Stand. No. 406 (Method 1042), Gen. Serv. Admin., Oct. 5, 1961. (Supersedes Fed. Specif. L-P-406b.)

8. Anon.: Standard Method of Test for Bearing Strength of Plastics. ASTM Designation: D 953-54. Pt. 27 of 1968 Book of ASTM Standards With Related Material. Amer. Soc. Testing Mater., 1968, pp. 391-397.

9. Anon.: Sandwich Constructions and Core Materials; General Test Methods. MIL-STD-401B, U.S. Dep. Def., Sept. 26, 1967. (Supersedes MIL-STD-401A.)

TABLE I.- FIBER-METAL SHEET TENSILE TEST RESULTS

[Material: AISI 347 stainless steel]

Specime	Mesh orientation deg	Dimensions, in		Area, in^2	Rayl	Fiber	tensity, lb/in^3	Load lb	Tensile stress, psi	Gage, in.	Elongation in.	Elongation percent
		T	W									
F1-1	0	0.047	1	1.047	31	C-28	0.151	778	16 500	2.19	0.250	11.4
F1-2	0	.047	1	.047	31	C-28	.151	822	17 500	2.19	.300	13.7
F1-3	0	.047	1	.047	31	C-28	.151	758	16 100	2.19	.300	13.7
F1-4	90	.047	1	.047	31	C-28	.151	807	17 200	2.16	.244	11.2
F1-5	90	.047	1	.047	31	C-28	.151	776	16 500	2.19	.268	12.2
F1-6	90	.047	1	.047	31	C-28	.151	770	16 400	2.19	.294	13.4
F1-7	45	.047	2	.094	31	C-28	.151	1489	15 900	2.13	.313	14.7
F1-8	45	.047	2	.094	31	C-28	.151	1600	17 000	2.06	.313	15.2
F1-9	45	.047	2	.094	31	C-28	.151	1532	16 300	2.13	.288	13.5
F2-1	0	0.049	1	1.049	78	C-28	0.176	1065	21 800	2.19	0.301	13.7
F2-2	0	.049	1	.049	78	C-28	.176	883	18 000	2.13	.206	9.7
F2-3	0	.049	1	.049	78	C-28	.176	941	19 200	2.03	.281	13.8
F2-4	90	.049	1	.049	78	C-28	.176	912	18 600	2.16	.238	11.0
F2-5	90	.049	1	.049	78	C-28	.176	990	20 200	2.16	.294	13.6
F2-6	90	.049	1	.049	78	C-28	.176	852	17 400	2.08	.253	12.2
F2-7	45	.049	2	.098	78	C-28	.176	1821	18 600	2.06	.288	14.0
F2-8	45	.049	2	.098	78	C-28	.176	1844	18 900	2.06	.278	13.5
F2-9	45	.049	2	.098	78	C-28	.176	1775	18 100	2.06	.294	14.2
F3-1	0	0.049	1	1.049	12	C-28	0.112	500	10 200	2.16	0.294	13.5
F3-2	0	.049	1	.049	12	C-28	.112	469	9 580	2.13	.281	13.2
F3-3	0	.049	1	.049	12	C-28	.112	485	9 900	2.19	.295	13.4
F3-4	90	.049	1	.049	12	C-28	.112	464	9 500	2.22	.271	12.2
F3-5	90	.049	1	.049	12	C-28	.112	483	9 870	2.19	.269	12.3
F3-6	90	.049	1	.049	12	C-28	.112	490	10 000	2.16	.274	12.7
F3-7	45	.049	2	.098	12	C-28	.112	793	8 000	2.19	.255	11.6
F3-8	45	.049	2	.098	12	C-28	.112	812	8 300	2.16	.269	12.4
F3-9	45	.049	2	.098	12	C-28	.112	600	6 120	2.16	.213	9.9
F4-2	0	0.041	1.020	1.0418	8	C-38	0.129	497	11 890	2.00	0.390	19.5
F4-3	0	.041	1.025	.042	8	C-38	.129	424	10 100	2.00	.325	16.3
F4-4	0	.041	1.019	.0417	8	C-38	.129	436	10 420	2.00	.295	14.8
F4-5	0	.041	.996	.0408	8	C-38	.129	462	11 310	2.00	.355	17.8
F4-6	0	.040	1.013	.0405	8	C-38	.129	486	12 000	2.00	.340	17.0
F4-7	0	.041	1.029	.0422	8	C-38	.129	464	11 000	2.00	.300	15.0
F4-8	0	.040	1.003	.040	8	C-38	.129	440	11 000	2.00	.350	17.5
F4-9	0	.041	1.001	.041	8	C-38	.129	454	11 050	2.00	.310	15.5
F5-1	0	0.049	0.985	1.0483	10	C-38	0.135	536	11 100	2.00	0.305	15.3
F5-2	0	.048	1.017	.0488	10	C-38	.135	552	11 300	2.00	.360	18.0
F5-3	0	.053	.984	.0521	10	C-38	.135	456	8 750	2.00	.305	15.3
F5-4	0	.051	.977	.0498	10	C-38	.135	552	11 080	2.00	.280	14.0
F5-5	0	.051	1.047	.0534	10	C-38	.135	612	11 480	2.00	.270	13.5
F5-6	0	.049	1.016	.0498	10	C-38	.135	546	10 960	2.00	.295	15.5

Specimen	Core density, lb/ft^3	Cell size, in.	Ultimate compressive load, lb	Compressive stress, psi
(-314	1.9	3/4	3340	93
(-3)5	1.9	3/4	3300	92
(-3)6	1.9	3/4	3210	89
(-5)4	1.6	1 1/8	2640	73
(-5)5	1.6	1 1/8	2200	61
(-5)6	1.6	1 1/8	2050	57
(-7)4	1.9	3/4	6640	184
(-7)5	1.9	3/4	6180	172
(-7)6	1.9.	3/4	6420	179
(-914	1.6	1 1/8	4660	130
(-9)5	1.6	1 1/8	4470	124
(-9)6	1.6	1 1/8	4900	136

TABLE III.- CORE AND ADHESIVE FLATWISE-TENSILE TEST RESULTS

[Heat-resistant, phenolic, fiber-glass-reinforced, sine-wave configuration]

Specimen	Core density, lb/ft^3	Cell size, in.	Adhesive	Adhesive weight, lb/ft^2 (**)	Film thickness, in. (**)	Area, in^2	Ultimate load, lb	Tensile stress, psi
(-3)1	1.9	3/4	X-10-95-3	----	----	36.0	12400	344
(-3)2	1.9	3/4	X-10-95-3	----	----	36.0	-----	---
(-313	1.9	3/4	X-10-95-3	----	----	36.0	8300	231
(-5)1	1.9	3/4	Narmco 328	0.075	0.008	36.0	11625	323
(-5)2	1.9	3/4	Narmco 328	.075	.008	36.0	14000	389
(-5)3	1.9	3/4	Narmco 328	.075	.008	36.0	14150	393
A3-1	4.5	3/8	Narmco 328	0.055	0.007	4.0	1085	271
A3-2	4.5	3/8	Narmco 328	.055	.007	4.0	1500	375
A3-3	4.5	3/8	Narmco 328	.055	.007	4.0	1470	368
A3-4	4.5	3/8	Narmco 328	.055	.007	4.0	1220	305
A3-5	4.5	3/8	Narmco 328	.055	.007	4.0	1280	320
A4-1	4.5	3/8	Narmco 328	0.110	0.014	4.0	1560	390
A4-2	4.5	3/8	Narmco 328	.110	.014	4.0	1445	361
A4-3	4.5	3/8	Narmco 328	.110	.014	4.0	1420	355
A4-4	4.5	3/8	Narmco 328	.110	.014	4.0	1490	373
A4-5	4.5	3/8	Narmco 328	.110	.014	4.0	1420	355
CT1-1*†	2.0	3/4	Narmco 328	0.110 / 0.055	0.014 / 0.007	36.0	11110	309
CT1-2*†	2.0	3/4	Narmco 328	0.110 / 0.055	0.014 / 0.007	36.0	10750	299
CT1-3*†	2.0	3/4	Narmco 328	0.110 / 0.055	0.014 / 0.007	36.0	11580	322
CT1-4*†	2.0	3/4	Narmco 328	0.110 / 0.055	0.014 / 0.007	36.0	11580	322
CT1-5*†	2.0	3/4	Narmco 328	0.110 / 0.055	0.014 / 0.007	36.0	12100	336
CT1-6*†	2.0	3/4	Narmco 328	0.110 / 0.055	0.014 / 0.007	36.0	11640	323
CT2-1*	2.0	3/4	Narmco 328	0.110 / 0.055	0.014 / 0.007	36.0	11460	318
CT2-2*	2.0	3/4	Narmco 328	0.110 / 0.055	0.014 / 0.007	36.0	13325	370
CT2-3*	2.0	3/4	Narmco 328	0.110 / 0.055	0.014 / 0.007	36.0	10000	278
CT2-4*	2.0	3/4	Narmco 328	0.110 / 0.055	0.014 / 0.007	36.0	11560	321
CT2-5*	2.0	3/4	Narmco 328	0.110 / 0.055	0.014 / 0.007	36.0	11150	310
CT2-6*	2.0	3/4	Narmco 328	0.110 / 0.055	0.014 / 0.007	36.0	14125	393

*Specimens which had adhesive failures.

†Specimens which have drain-hole grooves.

**Two values indicate different bond weights or thicknesses at upper and lower surfaces.

TABLE IV.- CORE- AND ADHESIVE-SHEAR TEST RESULTS

Feat-resistant, phenolic, fiber-glass-reinforced, sine-wave configuration

Specimen	Dimensions, in.			Direction of applied load	Applied load, lb	Shear area, in^2	Core density, lb/ft^3	Shear stress, psi	Shear modulus, psi	Cell size, in.
	L	W	T							
C3-1†	6	2	1/2	L	1450	12	1.9	120.9	2780	3/4
C3-2†	6	2	1/2	L	1464	12	1.9	122.Q	2380	3/4
c3-37	6	2	1/2	L	1713	12	1.9	142.9	2780	3/4
C4-1†	2	6	1/2	W	1097	18	1.9	60.9	1279	3/4
C4-2†	2	6	1/2	W	1114	18	1.9	62.0	1139	3/4
C4-3*†	2	6	1/2	W	813	18	1.9	----	----	3/4
C4-47	2	6	1/2	W	1288	18	1.9	71.5	1220	3/4
C4-57	2	6	1/2	W	1280	18	1.9	71.2	1280	3/4
C4-6†	2	6	1/2	W	1236	18	1.9	68.7	1170	3/4
C4-77	2	6	1/2	W	1180	18	1.9	65.6	1110	3/4
C4-8†	2	6	1/2	W	1186	18	1.9	65.9	1289	3/4
C4-97	2	6	1/2	W	1248	18	1.9	69.4	1229	3/4
C4-10†	2	6	1/2	W	1176	18	1.9	65.4	1160	3/4
C4-11†	2	6	1/2	W	1241	18	1.9	69.0	980	3/4
C4-12†	2	6	1/2	W	1280	18	1.9	71.1	1210	3/4
C4-13†	2	6	1/2	W	1088	18	1.9	60.4	1036	3/4
C4-14†	2	6	1/2	W	1304	18	1.9	72.5	1250	3/4
C4-15†	2	6	1/2	W	1168	18	1.9	64.8	1062	3/4
C2-6	2	6	1/2	W	1188	18	1.9	65.8	1310	3/4
C2-7	2	6	1/2	W	1092	18	1.9	60.7	1332	3/4
C2-8	2	6	1/2	W	1284	18	1.9	71.4	1139	3/4
C2-9	2	6	1/2	W	1289	18	1.9	71.6	1059	3/4
c2-10	2	6	1/2	W	1366	18	1.9	75.9	1069	3/4
c2-11	2	6	1/2	W	1347	18	1.9	74.8	1307	3/4
c2-12	2	6	1/2	W	1283	18	1.9	71.4	1110	3/4
C2-13	2	6	1/2	W	1304	18	1.9	72.5	1435	3/4
C2-14	2	6	1/2	W	1428	18	1.9	79.4	1852	3/4
C2-15	2	6	1/2	W	1266	18	1.9	70.3	1685	3/4
CS5-1†	8	3	1/2	L	3650	24	2.0	152.0	1768	3/4
CS5-2†	8	3	1/2	L	3130	24	2.0	130.2	1714	3/4
CS5-37	8	3	1/2	L	3400	24	2.0	141.8	1609	3/4
CS5-47	8	3	1/2	L	3240	24	2.0	135.0	1609	3/4
CS5-57	8	3	1/2	L	3450	24	2.0	143.8	1595	3/4
CS5-6†	8	3	1/2	L	3120	24	2.0	130.0	1547	3/4
CS5-77	8	3	1/2	L	3460	24	2.0	144.2	1500	3/4
CS5-8†	8	3	1/2	L	3270	24	2.0	136.2	1620	3/4
CS5-97	8	3	1/2	L	3370	24	2.0	140.3	1595	3/4
CS5-10†	8	3	1/2	L	2870	24	2.0	119.5	1660	3/4

†Specimens which have drain-hole grooves.

*All failures were core shear except that for C4-3, which was an adhesive failure.

TABLE V. - SYMMETRICAL HONEYCOMB SANDWICH FLEXURAL TEST RESULTS

[Static quarter-point loading; honeycomb core – HRP 3/4 GF14-1.9; adhesive – Narmco 328]

Specimen	Top face skin	Bottom face skin	Ultimate load, lb	Elongation, in.	Type of failure	EI of sandwich, lb-in^2
SS1-1	FM-119	FM-119	187	0.295	Face wrinkle	29 100
		FM-119	199	.230	Core shear	39 600
		FM-119	203	.238	Adhesive shear	39 100
SS1-4	FM-119	FM-119	227	.36	Face wrinkle	28 900
SS2-1	FM-121	FM-121	222	0.45	Core crushed	22 600
SS2-2	FM-121	FM-121	159	.329	Core shear	22 150
SS2-3	FM-121	FM-121	150	.173	Core shear	39 800
SS2-4	FM-121	FM-121	199	.42	Core crushed	21 700

TABLE VI.- SYMMETRICAL SANDWICH FLEXURAL-FATIGUE TEST RESULTS

All specimens used fiber-glass HRP 3/4 GF14-1.9 honeycomb core (ungrooved). One layer of Narmco 328 adhesive was used to bond both faces of the honeycomb core to the porous facings of all specimens. Gage of all facing sheets is 0.040 inch.

Specimen	Top face skin	Bottom face skin	Maximum facing stress, psi	Minimum facing stress, psi	Stress ratio, R	Alternating stress range, psi	Mean stress, psi	Ultimate stress, psi	Cycles to failure	Type of failure
SS1-12	FM-119	FM-119	7940	1980	0.25	5960	4960	11 000	47 000	Tension
SS1- 5	FM-119	FM-119	7940	1980	.25	5960	4960	11 000	35 000	Tension
SS1-13	FM-119	FM-119	----	----	----	----	----	-----	----	Delaminated
SS1- 9	FM-119	FM-119	5950	1980	.333	3970	3965	11 000	93 000	Tension
SS1-10	FM-119	FM-119	5950	1980	.333	3970	3965	11 000	179 000	Tension
SS1-11	FM-119	FM-119	5950	1980	.333	3970	3965	11 000	98 000	Tension
SS1- 6	FM-119	FM-119	3970	1980	.50	1990	2975	11 000	2 620 000	Tension
SS1- 7	FM-119	FM-119	3970	1980	.50	1990	2975	11 000	10 320 000	No failure
SS1- 8	FM-119	FM-119	3970	1980	.50	1990	2975	11 000	3 166 000	Tension
SS2-12	FM-121	FM-121	7940	1980	0.25	5960	4960	10 500	15 000	Tension
SS2-13	FM-121	FM-121	7940	1980	.25	5960	4960	10 500	13 000	Tension
SS2-14	FM-121	FM-121	7940	1980	.25	5960	4960	10 500	29 000	Tension
SS2- 9	FM-121	FM-121	5950	1980	.333	3970	3965	10 500	41 000	Tension
SS2-10	FM-121	FM-121	5950	1980	.333	3970	3965	10 500	71 000	Tension
SS2-11	FM-121	FM-121	5950	1980	.333	3970	3965	10 500	53 000	Tension
SS2- 6	FM-121	FM-121	3970	1980	.50	1990	2975	10 500	1 317 000	Tension
SS2- 7	FM-121	FM-121	3970	1980	.50	1990	2975	10 500	460 000	Compression
SS2- 8	FM-121	FM-121	3970	1980	.50	1990	2975	10 500	892 000	Tension

TABLE VII.- MECHANICAL JOINT EVALUATION, SANDWICH-BEAM FLEXURAL TEST RESULTS

(a) Fan-duct wall simulation

Single-sandwich construction:
Top face skin - FM-121
Bottom face skin - 1/4-inch fiber glass
Honeycomb core - HRP 3/4 GF14-1.9
Adhesive - Narmco 328

Specimen	Initial failure load, lb	Deflection, in.	Type of failure
J1-1W	550	0.0678	Flatwise tensile of adhesive, core to fiber glass
J1-2W	860	.1148	
J1-3W	880	.095	
J1-4W	600	.110	
J1-5W	920	.155	

(b) Splitter simulation

Double-sandwich construction:
Top and bottom face skin - FM-121
Center face skin - 0.020 corrosion-resistant sheet, type 321 stainless steel
Honeycomb core - HRP 3/4 GF14-1.9
Adhesive - Narmco 328

Specimen	Yield load, lb	Deflection due to yield load, in.	Ultimate load, lb	Deflection due to ultimate load, in.	Type of failure
J1-1S	1840	0.100	3100	0.330	Rivet shear
J1-2S	1350	.675	2750	.235	Rivet shear
51-35	1750	.835	3000	.292	Rivet shear
J1-4S	1915	.910	2900	.295	Rivet shear
J1-5S	1810	.760	2775	.210	Rivet shear

48" TREATED FAN EXHAUST DUCT AND TWO-CONCENTRIC-RING TREATED INLET

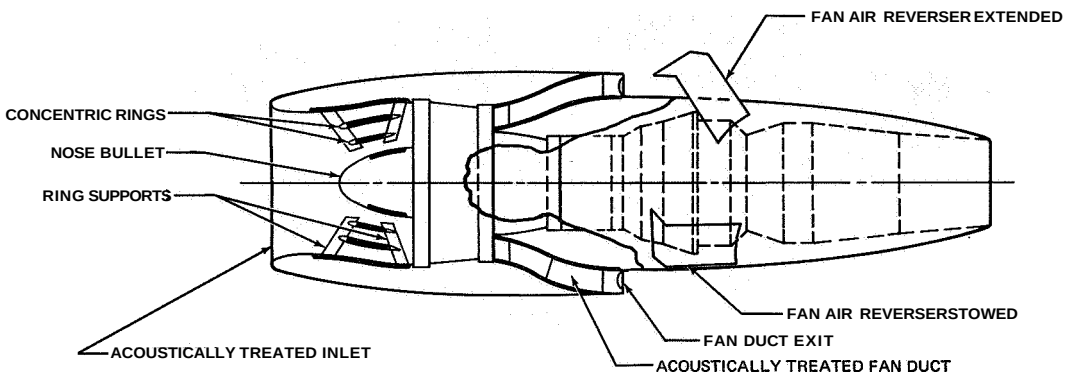

Figure 1

ACOUSTICAL DUCT-LINING COMPONENTS

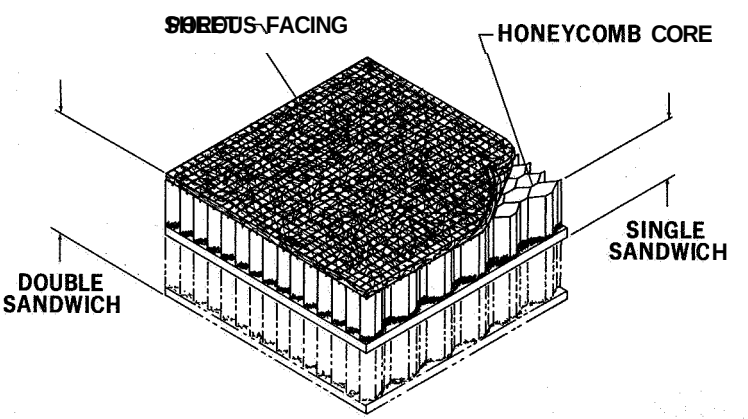

Figure 2

ACOUSTICAL-SANDWICH COMPONENTS

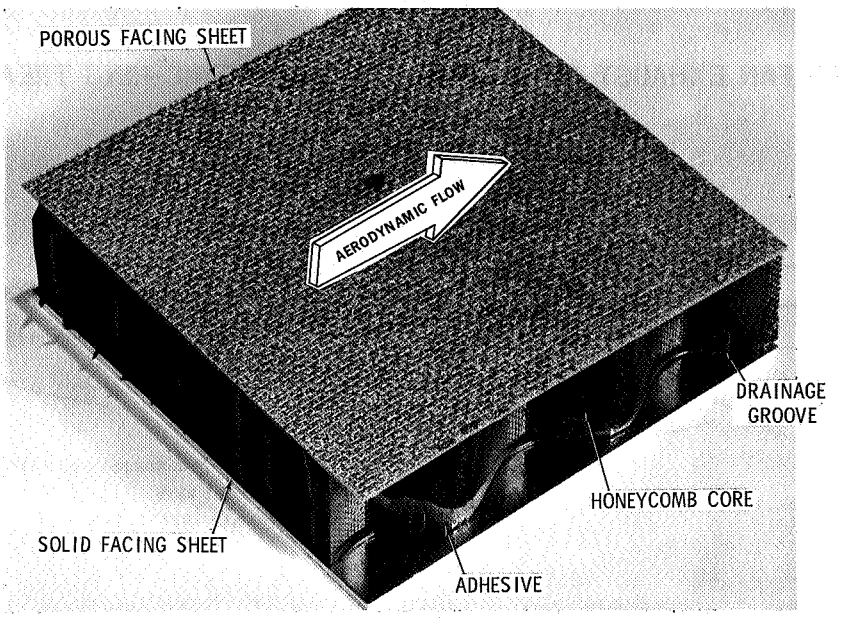

Figure 3 L-68-8546

EXAMPLE OF PERFORATED SHEET

Figure 4 L-68-8547

TYPICAL POROUS SHEET CONFIGURATIONS

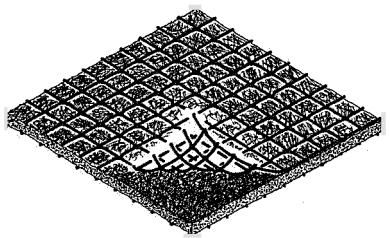

SINTERED FIBER METAL

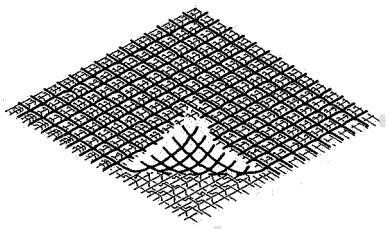

SINTERED WOVEN WIRE

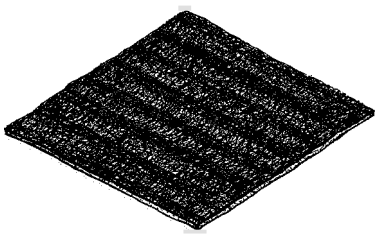

SINTERED CONTINUOUS FILAMENT

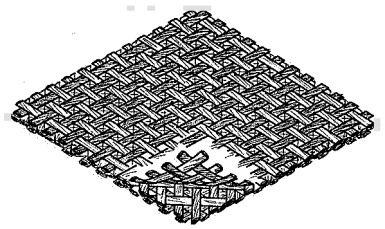

WOVEN FIBER GLASS

Figure 5

FIBER-METAL MICROGRAPH CROSS SECTION - 10 RAYL

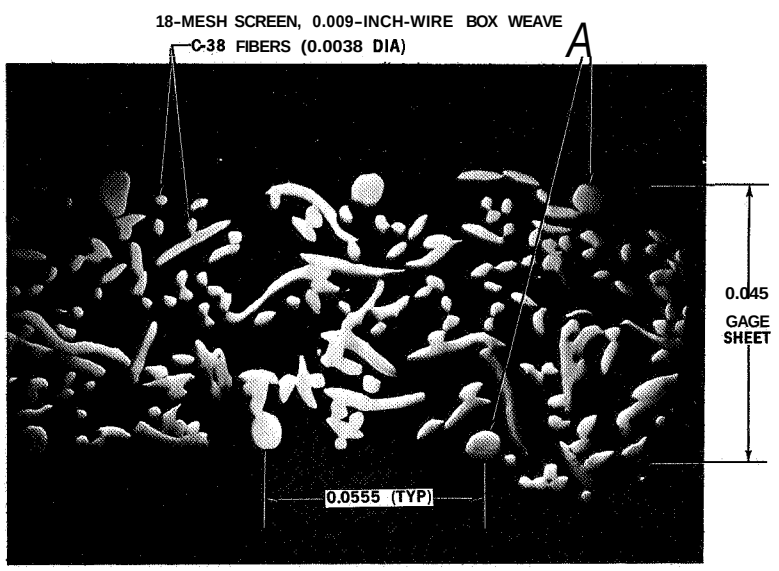

Figure 6

L-68-8548

TYPICAL POROUS-SHEET–CORE INTERFACE

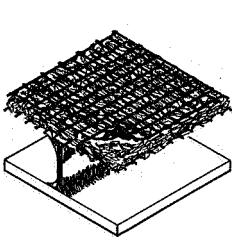

FIBER METAL BONDED TO FIBER-GLASS CORE

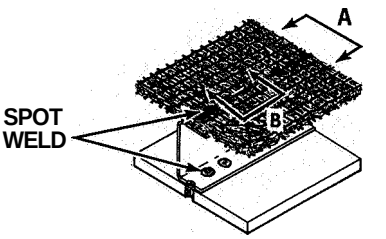

FIBER METAL OR SCREEN WELDED TO METAL CORE

INTERWOVEN STRUCTURE (RESIN SYSTEM OMITTED)

Figure 7

MICROGRAPHIC STUDY OF BONDED INTERFACE

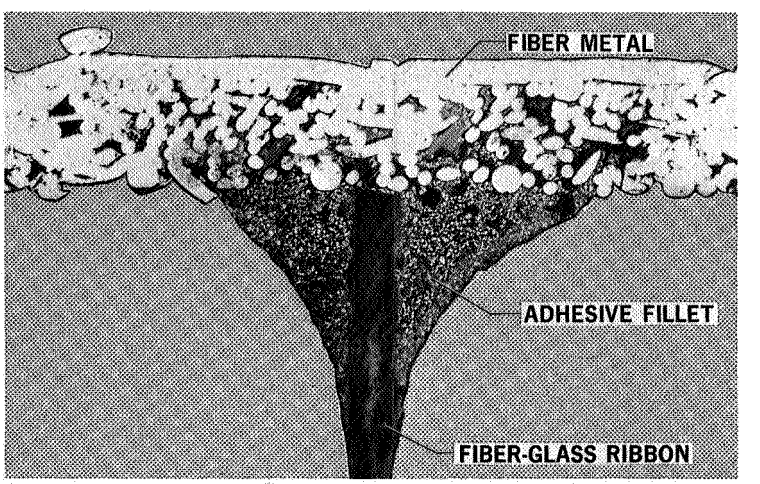

Figure 8

L-68-8541

EXPLODED VIEW OF TYPICAL ACOUSTIC-SANDWICH MATERIALS

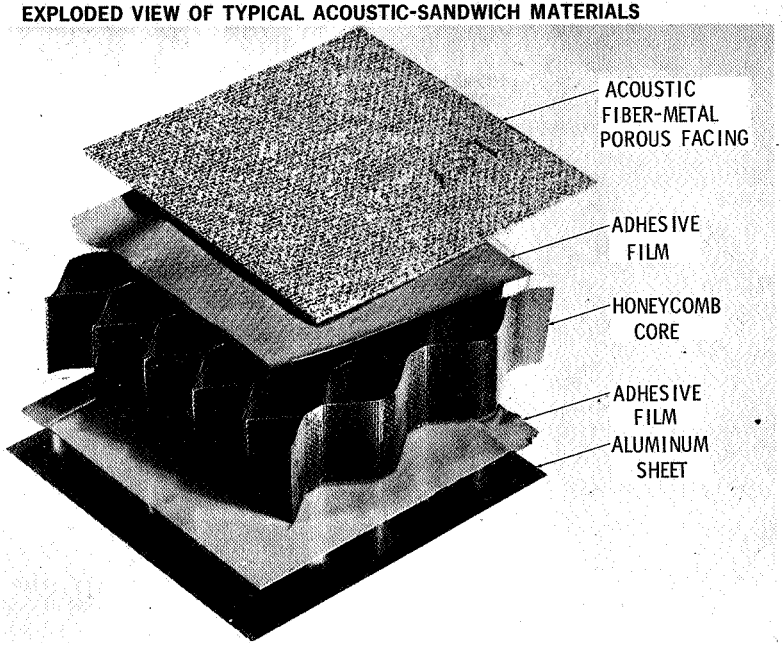

Figure 9

L-68-8549

ACOUSTIC-SANDWICH BONDING PROCESS

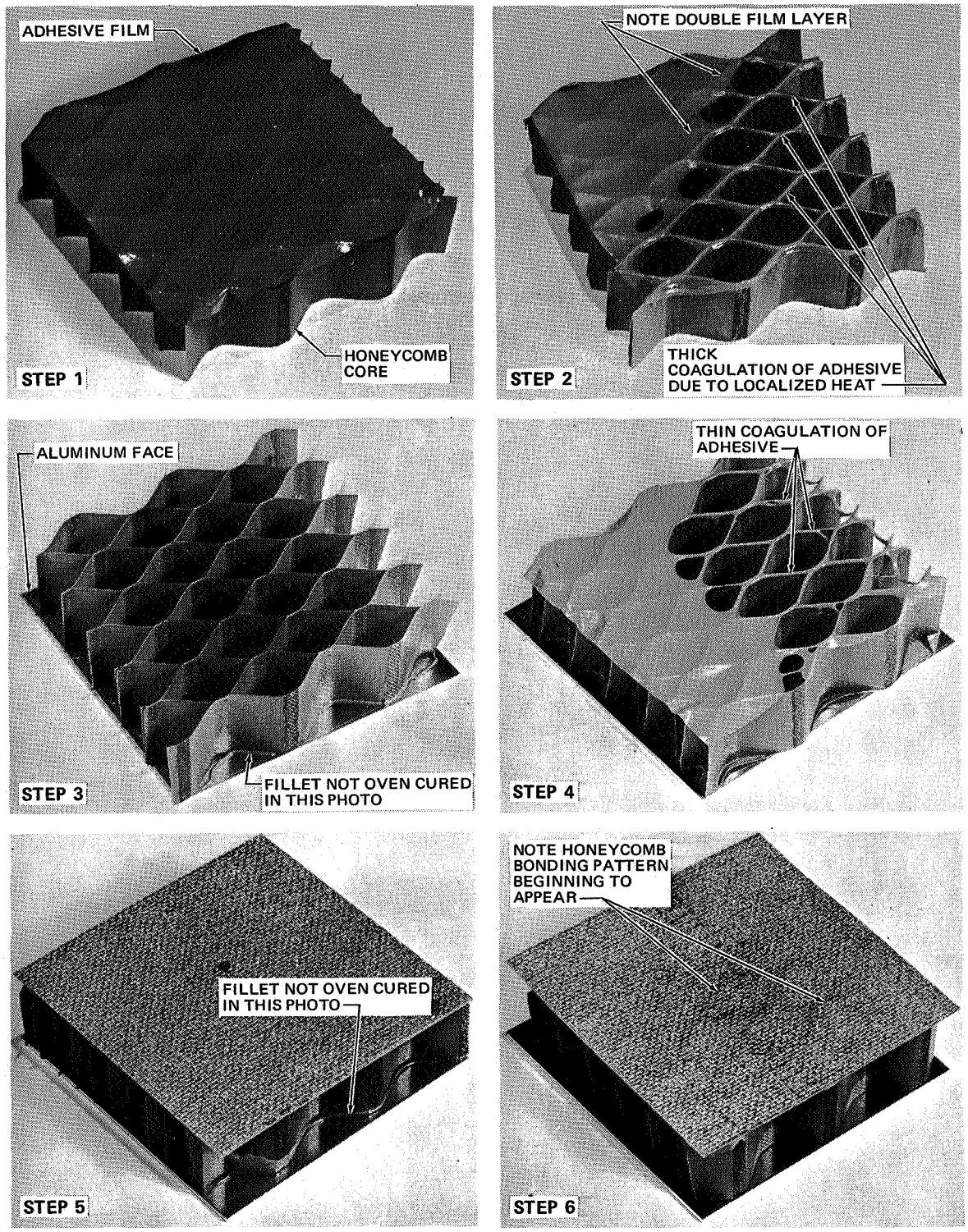

Figure 10 L-68-8550

MICROGRAPHIC STUDY OF WELDED INTERFACE
SECTION A

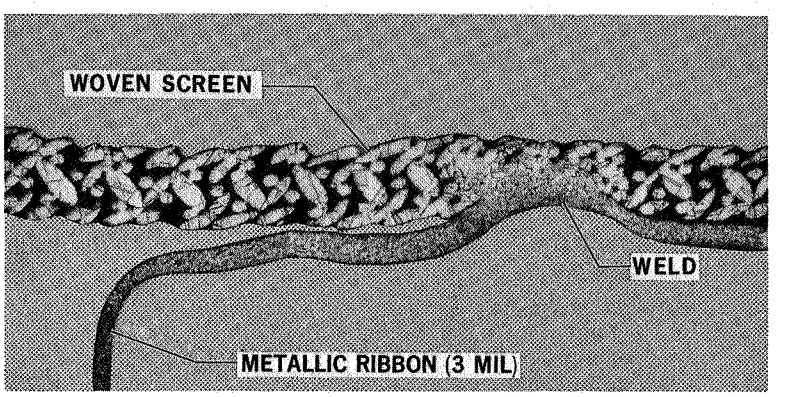

Figure 11 L-68-8542

MICROGRAPHIC STUDY OF WELDED INTERFACE
SECTION B

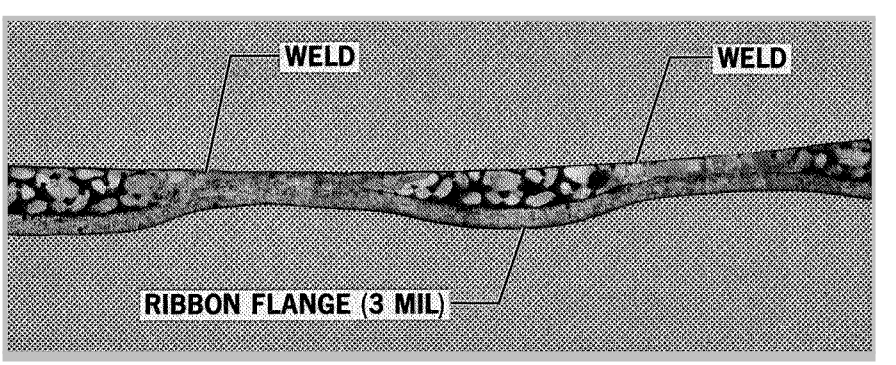

Figure 12 L-68-8551

TYPICAL TIME - OPERATION HISTORY

AIRCRAFT CONTAMINATION EXPOSURE OF ACOUSTIC LINER

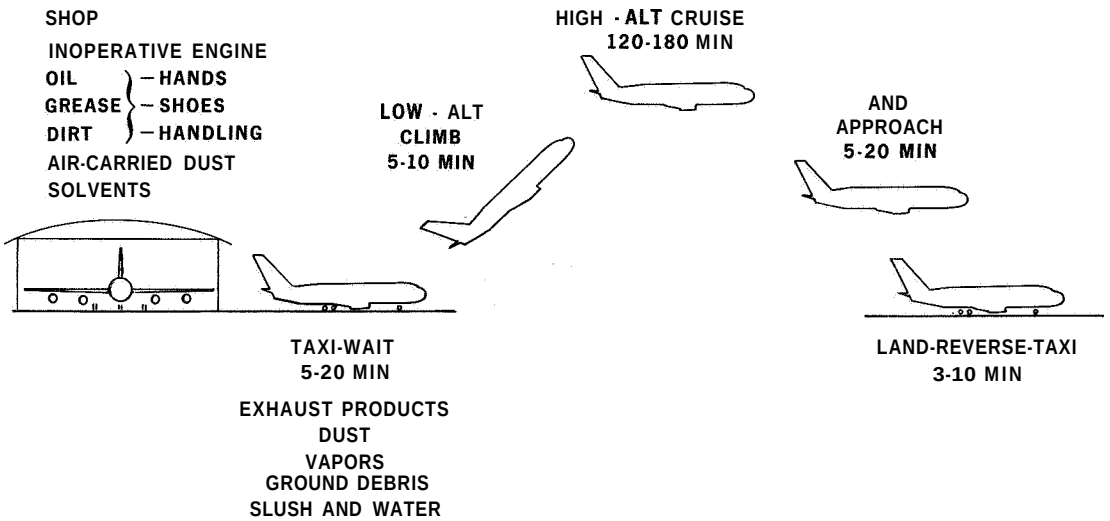

Figure 13

POLAR ORIENTATION PLOT OF FIBER-METAL TENSILE STRENGTH

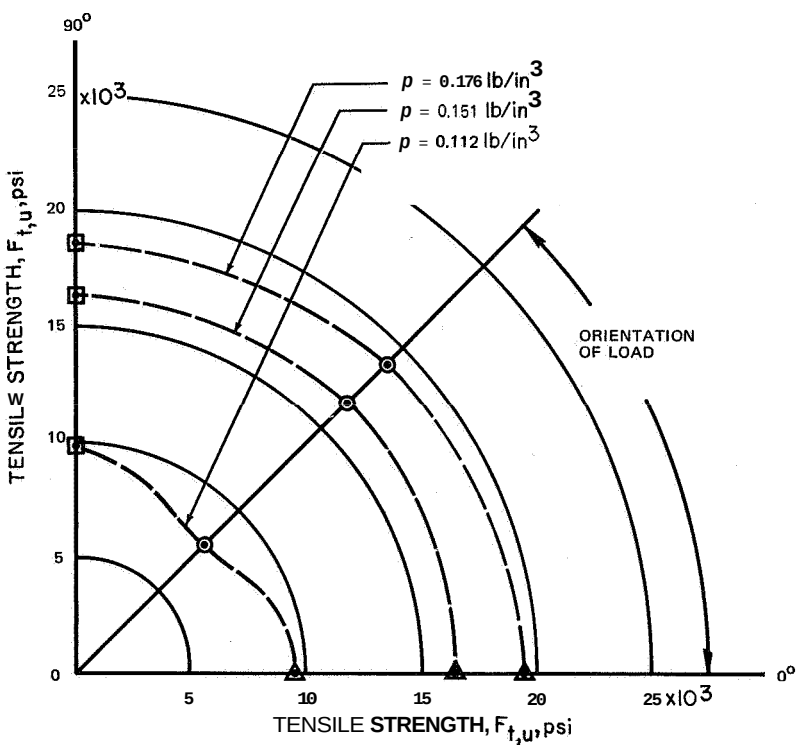

Figure 14

TYPICAL STRESS-STRAIN CURVE
POROUS FACING SHEET MATERIAL:

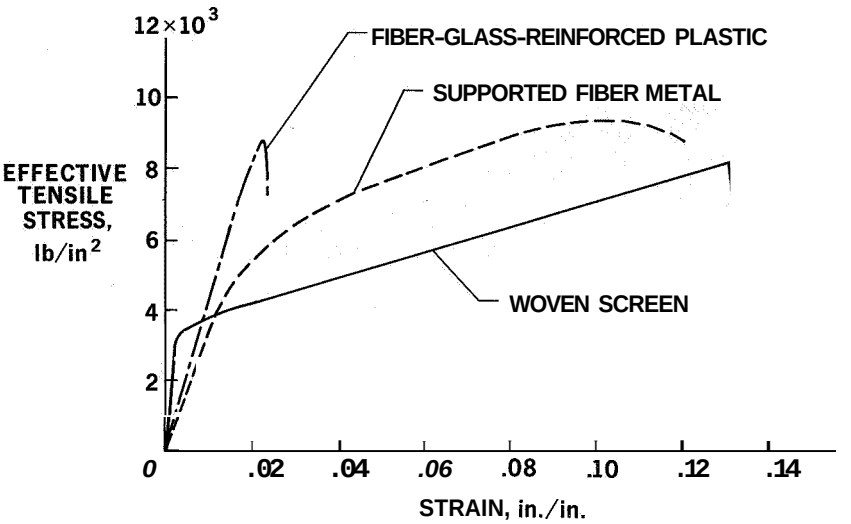

Figure 15

FLEXURAL-FATIGUE ELECTRODYNAMIC SHAKER

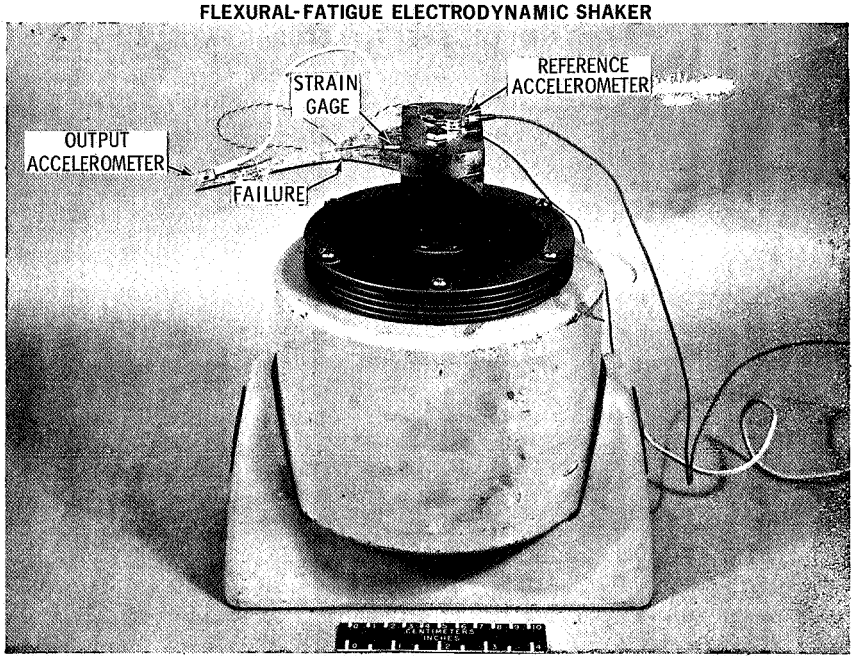

Figure 16 L-68-8552

FLEXURAL-FATIGUE TEST SPECIMEN

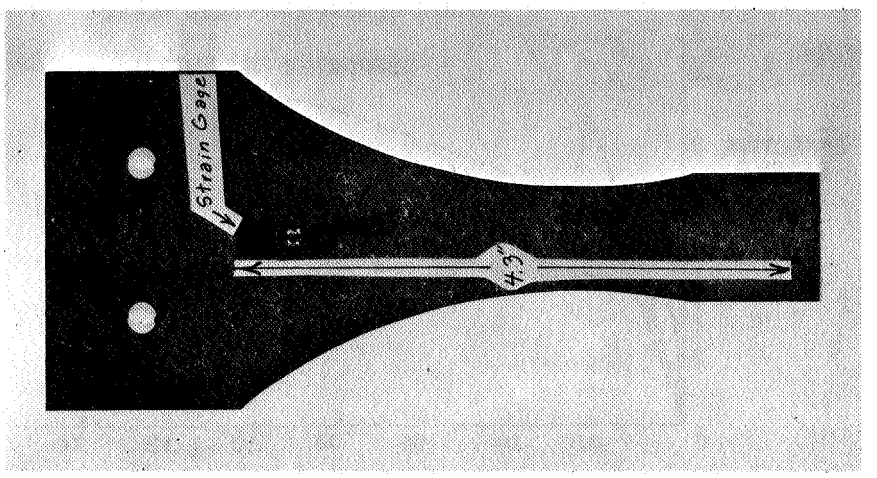

Figure 17 L-68-8553

S-N CURVE
FIBER-METAL SHEET; FLEXURAL FATIGUE

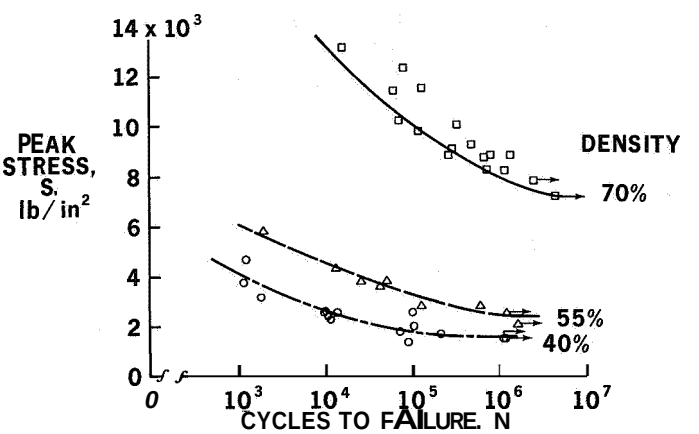

Figure 18

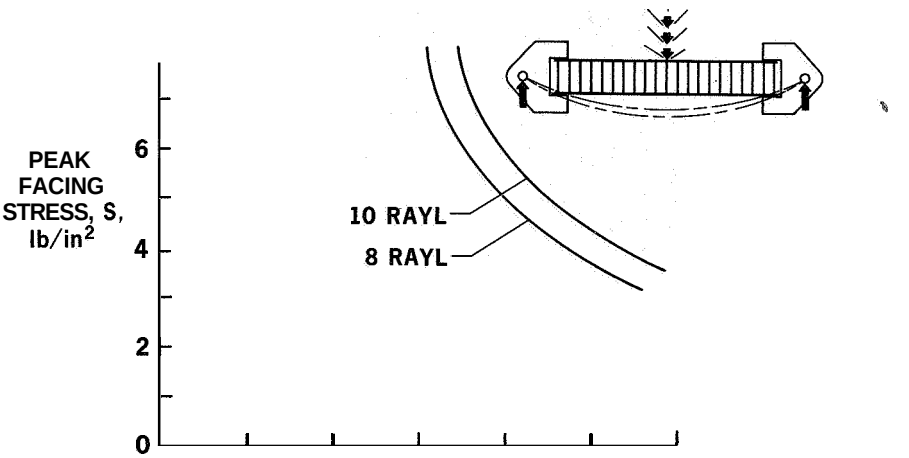

Figure 19

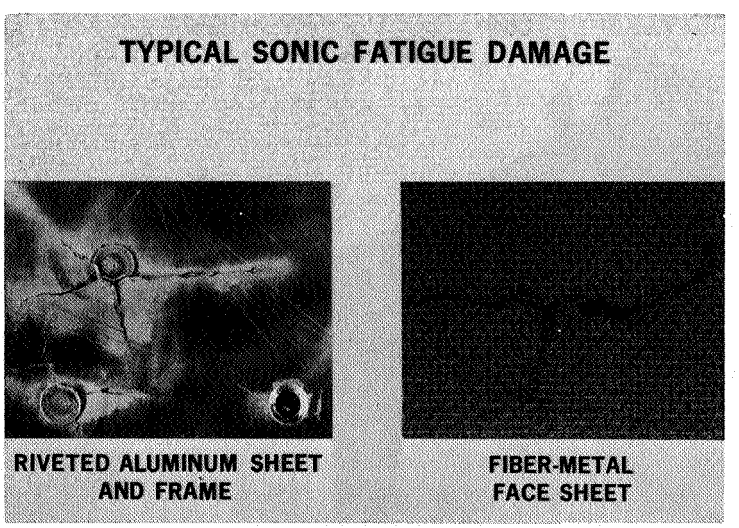

Figure 20 L-68-8543

INTERIOR OF CONTAMINATION TEST FIXTURE

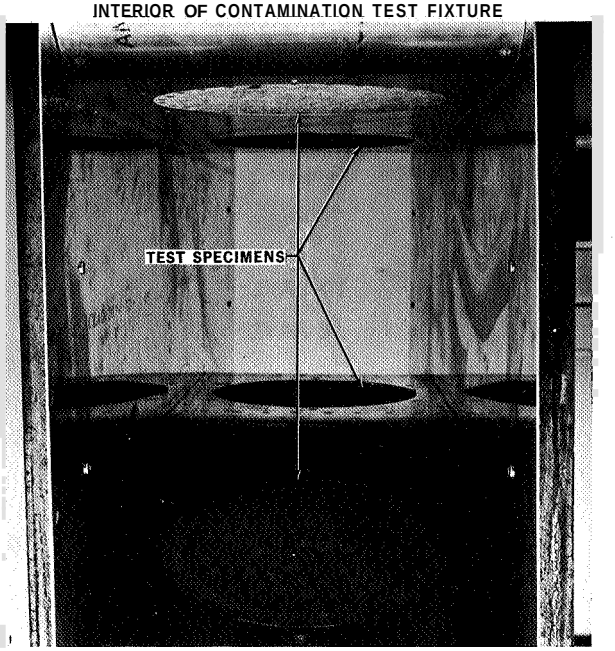

Figure 21 L-68-8554

CONTAMINATION TEST FIXTURE

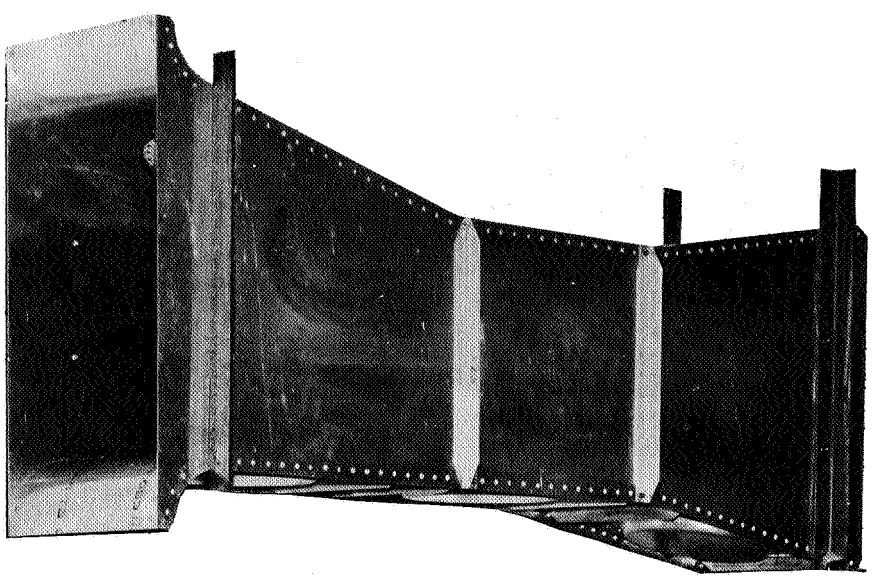

Figure 22 L-68-8600

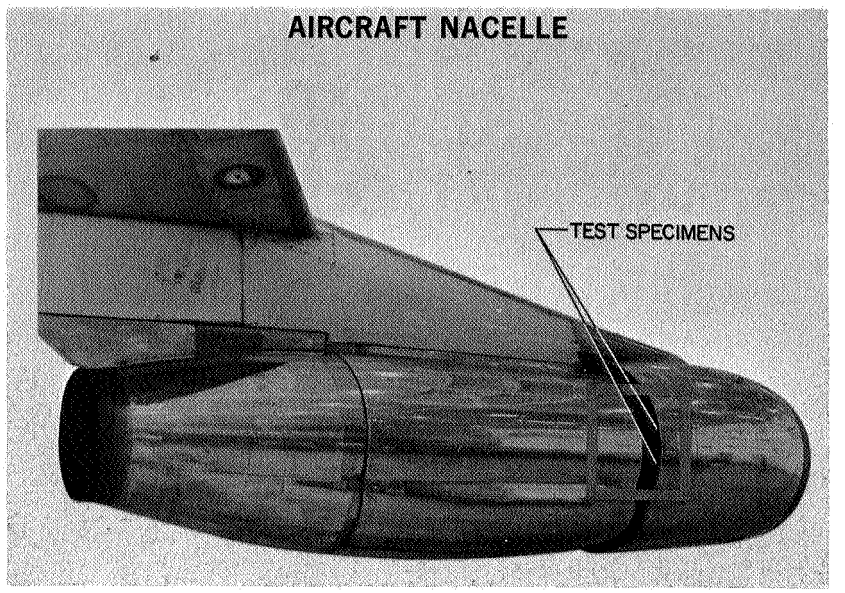

Figure 23 L-68-8544

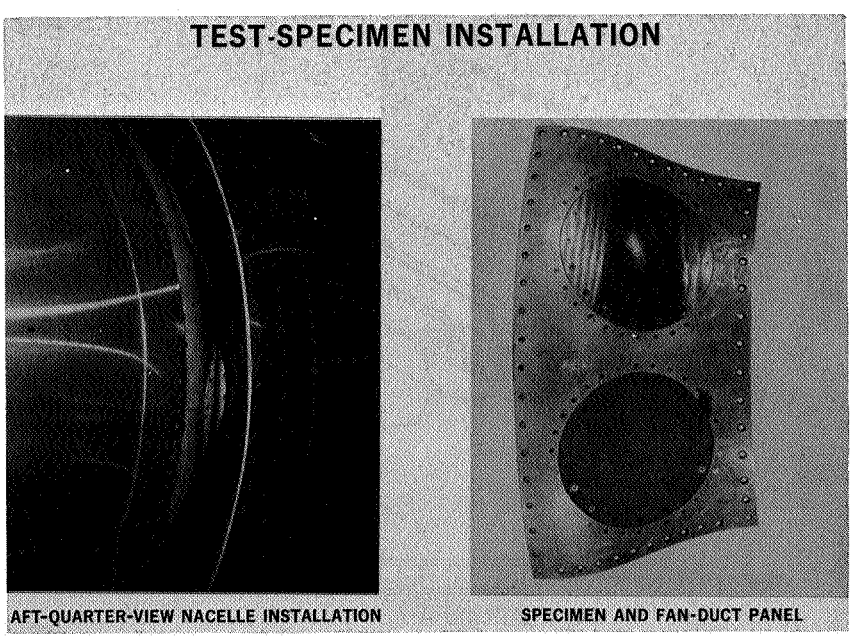

Figure 24 L-68-8545

CLOSEUP OF TEST SPECIMEN

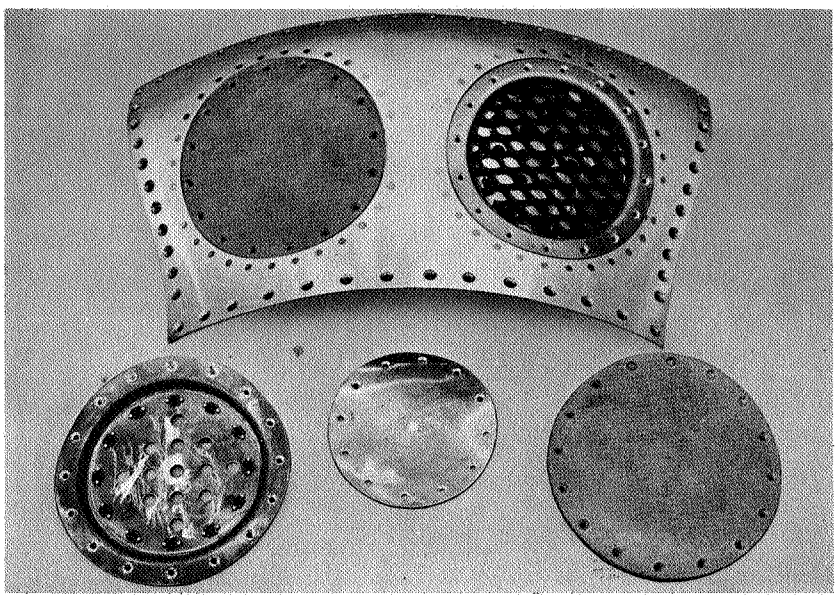

Figure 25 L-68-8555

DRAINAGE TEST FIXTURE

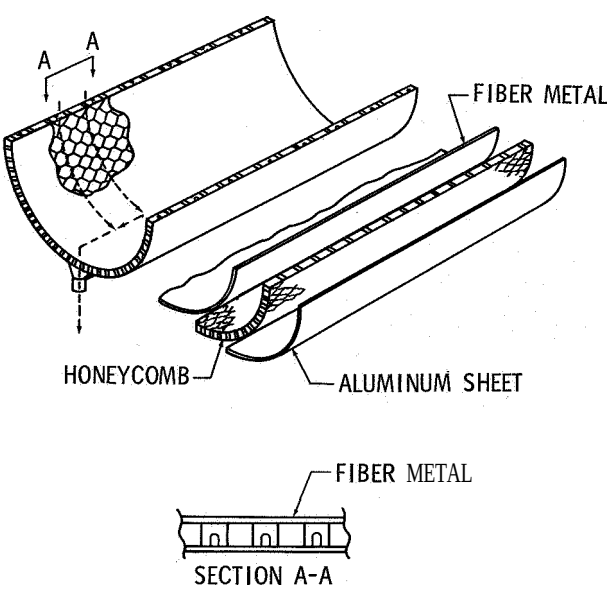

Figure 26

ACOUSTIC-PANEL BURNTHROUGH TEST; 2000° F FLAME

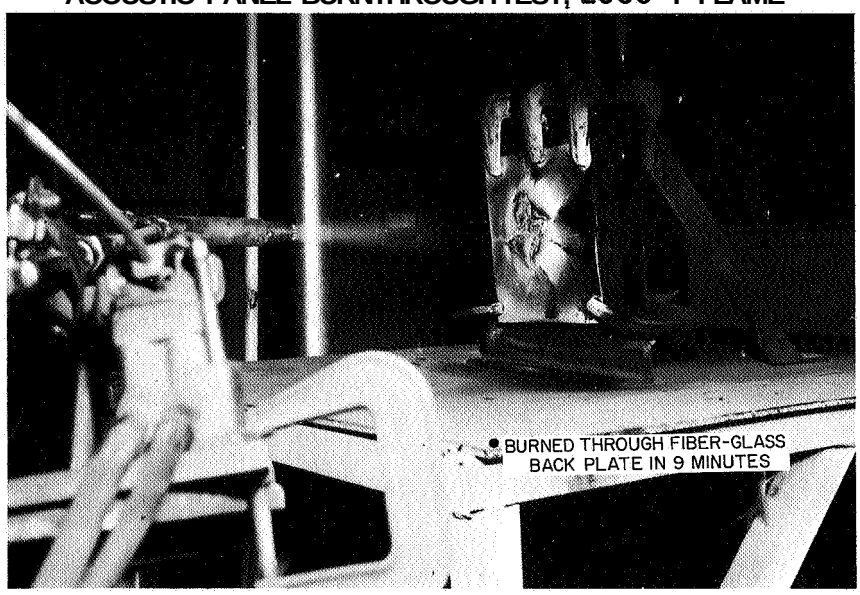

Figure 27 L-68-8556